


















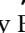



Disease surveillance by artificial intelligence links eelgrass wasting disease to ocean warming across latitudes

Lillian R. Aoki ^{1*,a,†} Brendan Rappazzo ^{2,†} Deanna S. Beatty ³ Lia K. Domke ⁴ Ginny L. Eckert ⁴
Morgan E. Eisenlord ¹ Olivia J. Graham ¹ Leah Harper ⁵ Timothy L. Hawthorne ⁶
Margot Helsing-Lewis ⁷ Kevin A. Hovel ⁸ Zachary L. Monteith ⁷ Ryan S. Mueller ⁹
Angeleen M. Olson ⁷ Carolyn Prentice ⁷ John J. Stachowicz ³ Fiona Tomas ¹⁰ Bo Yang ^{6,b}
J. Emmett Duffy ⁵ Carla Gomes ^{2,*} C. Drew Harvell ^{1*}

¹Department of Ecology and Evolutionary Biology, Cornell University, Ithaca, New York

²Department of Computer Science, Cornell University, Ithaca, New York

³Department of Evolution and Ecology, University of California, Davis, California

⁴College of Fisheries and Ocean Sciences, University of Alaska Fairbanks, Juneau, Alaska

⁵Tennenbaum Marine Observatories Network, Smithsonian Institution, Edgewater, Maryland

⁶Department of Sociology and College of Sciences GIS Cluster, University of Central Florida, Orlando, Florida

⁷Hakai Institute, Heriot Bay, British Columbia, Canada

⁸Department of Biology, Coastal & Marine Institute, San Diego State University, San Diego, California

⁹Department of Microbiology, Oregon State University, Corvallis, Oregon

¹⁰Instituto Mediterraneo de Estudios Avanzados (UIB-CSIC), Esporles, Spain

Abstract

Ocean warming endangers coastal ecosystems through increased risk of infectious disease, yet detection, surveillance, and forecasting of marine diseases remain limited. Eelgrass (*Zostera marina*) meadows provide essential coastal habitat and are vulnerable to a temperature-sensitive wasting disease caused by the protist *Labyrinthula zosterae*. We assessed wasting disease sensitivity to warming temperatures across a 3500 km study range by combining long-term satellite remote sensing of ocean temperature with field surveys from 32 meadows along the Pacific coast of North America in 2019. Between 11% and 99% of plants were infected in individual meadows, with up to 35% of plant tissue damaged. Disease prevalence was 3× higher in locations with warm temperature anomalies in summer, indicating that the risk of wasting disease will increase with climate warming throughout the geographic range for eelgrass. Large-scale surveys were made possible for the first time by the Eelgrass Lesion Image Segmentation Application, an artificial intelligence (AI) system that quantifies eelgrass wasting disease 5000× faster and with comparable accuracy to a human expert. This study highlights the value of AI in marine biological observing specifically for detecting widespread climate-driven disease outbreaks.

Disease outbreaks frequently cause rapid declines of host populations, transforming community structure and ecosystem functioning. Outbreaks that affect foundation or keystone species have particularly widespread and long-lasting

consequences. Prominent examples include the ecological extinction of chestnut trees in eastern U.S. forests from chestnut blight (Ellison et al. 2005); decimation of at least 20 species of sea-stars in the eastern Pacific due to sea-star wasting disease (Hewson

*Correspondence: lra53@cornell.edu; gomes@cs.cornell.edu; cdh5@cornell.edu

This is an open access article under the terms of the [Creative Commons Attribution](#) license, which permits use, distribution and reproduction in any medium, provided the original work is properly cited.

Additional Supporting Information may be found in the online version of this article.

^aPresent address: Data Science Initiative, University of Oregon, Eugene, Oregon

^bPresent address: Department of Urban and Regional Planning, San Jose State University, San Jose, California

Author Contribution Statement: J.E.D., C.D.H., J.J.S., T.L.H., and C.G. conceptualized the study, with contributions from L.R.A., B.R., M.E.E., O.J.G., M.H., K.A.H., F.T., and G.L.E. B.R. and C.G. developed the AI approach, L.R.A., D.S.B., L.D., G.L.E., M.E.E., O.J.G., L.H., C.D.H., M.H., K.A.H., Z.L.M., R.S.M., A.M.O., C.P., J.J.S., F.T., B.Y. collected data. L.R.A. and B.R. conducted analyses with input from C.D.H., J.E.D., J.J.S., C.G., M.H., M.E.E., B.Y., and T.L.H. L.R.A. and B.R. drafted the manuscript and all authors contributed to the final manuscript. L.R.A. and B.R. contributed equally to the manuscript.

[†]Shared first-authorship

et al. 2014); and vast reduction of reef-building corals throughout the Caribbean due to white-band disease (Aronson and Precht 2001). These outbreaks fundamentally reshaped ecosystems, with enduring impacts on human communities, yet timely monitoring of disease to identify outbreaks and inform management is limited. New methodologies are needed to alert managers to disease outbreaks across geographies that vary widely in environmental conditions, species characteristics, and human capacity to observe disease (Burge et al. 2014; Groner et al. 2016). Here, we investigate the relationship between warming climate and disease across 23° of latitude by harnessing advances in artificial intelligence (AI) to develop a novel and exponentially faster approach to disease detection in seagrass ecosystems.

Seagrasses are foundation species of highly productive coastal habitats that support fisheries, harbor biodiversity, filter pollutants, protect shorelines, and sequester carbon (UNEP 2020). Eelgrass (*Zostera marina*), a globally distributed species that is the dominant seagrass in temperate North America, is vulnerable to eelgrass wasting disease, caused by the protist *Labyrinthula zosterae*. Wasting disease infections occur when the pathogen enters eelgrass cells and consumes the chloroplasts; severe infections can cause shoot mortality (Short et al. 1987). Wasting disease outbreaks have contributed to ecologically damaging loss of seagrass during the last century, including extensive declines throughout North Atlantic coasts in the 1930s (Sullivan et al. 2013). Since *L. zosterae* was identified as the causative agent of wasting disease (Muehlstein et al. 1991), the eelgrass-*L. zosterae* pathosystem has been widely studied (Sullivan et al. 2013; Groner et al. 2016; Brakel et al. 2019; Jakobsson-Thor et al. 2020). Nevertheless, the drivers of wasting disease across the global distribution of eelgrass are poorly understood and surveillance is limited, in part due to the effort involved in confirming disease. Eelgrass wasting disease can be identified by characteristic dark-rimmed lesions on the leaf tissue, which to a trained eye are visually distinct from other damage such as desiccation (Fig. 1) (Sullivan et al. 2013, 2018). The presence of *L. zosterae* can be further verified with microscopy, culturing, and/or quantitative PCR (qPCR) (Bockelmann et al. 2013; Groner et al. 2016; Yoshioka et al. 2019). However, identification and quantification of lesion area are laborious and rely on specialized expertise, complicating surveillance at scales relevant to management and limiting our ability to forecast outbreaks or develop mitigation measures.

Warming ocean temperatures increase the urgency of developing scalable wasting disease detection methods to facilitate study of wasting disease sensitivity to temperature in the field. Eelgrass wasting disease infections peak during warm summer months (Bockelmann et al. 2013), and short-term warming events of < 5°C can negatively impact eelgrass growth (Reynolds et al. 2016), yet how warming temperatures may increase the risk of disease is not well understood. Warmer temperatures likely contributed to the 1930s outbreak (Sullivan et al. 2013), while regional surveys have shown that higher infection rates are also associated with longer plant leaves, higher shoot densities, and increased epiphyte loads, possibly

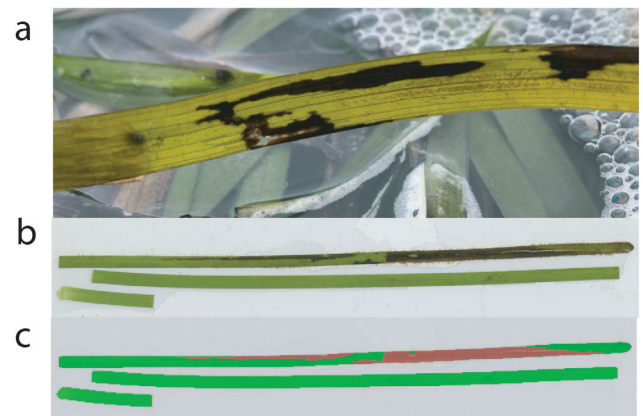


Fig. 1. Images of eelgrass leaves. **(a)** Eelgrass leaf with a wasting disease lesion, image credit: O. Graham. **(b)** Scanned image of a diseased eelgrass leaf. **(c)** Image segmentation mask produced by EeLISA, identifying healthy tissue in bright green and diseased tissue in red.

due to increased direct transmission in dense meadows and increased shading from epiphytes (Groner et al. 2016). Determining the generality of the temperature sensitivity of wasting disease across the geographic, morphological, and environmental variation known for eelgrass is critical to understand the impact of warming temperatures on disease risk.

Here, we determined the wasting disease status of eelgrass meadows across 23° of latitude (Fig. 2), and we leveraged long-term records of sea surface temperature (SST) to assess the sensitivity of eelgrass wasting disease to warming. Large-scale surveys were made possible for the first time by the Eelgrass Lesion Image Segmentation Application (EeLISA), an AI system that we developed to facilitate robust and standardized detection of eelgrass wasting disease (Rappazzo et al. 2021). EeLISA harnesses a convolutional neural network (CNN) for image segmentation and human-computer interaction for expert feedback (Fig. 3). Using EeLISA, we surveyed eelgrass wasting disease in 32 eelgrass meadows distributed across 3500 km of the Pacific coast of North America (Supporting Information Table S1). We used this dataset to investigate the effects of warming temperatures and plant and meadow characteristics on disease metrics across a wide range of eelgrass morphologies, environmental conditions, and levels of disease.

Materials and methods

Study sites

We sampled eelgrass meadow sites in six regions from 32°N to 55°N along the west coast of North America. (Fig. 2). We identified regions using abbreviations for the local state/province (AK, Alaska; BC, British Columbia; WA, Washington; OR, Oregon) except for in California, where we differentiated two regions by the local city where sampling occurred (BB, Bodega Bay; SD, San Diego). We sampled five meadows per region except in AK and BB where we sampled six meadows. We selected meadow sites based on the presence of intertidal



Fig. 2. Map of study sites and representative images of eelgrass meadows from each region. Study sites were located in six regions, distributed across 23° of latitude; see text for region codes. Image credit: B. Yang and L. Reshitnyk.

eelgrass, accessible at low tide by foot, and strong marine influence (salinity > 25 ppt in mid-summer, Supporting Information Table S1). Meadow sites within regions were located in distinct embayments or in distinct areas of seagrass within a larger embayment and separated by a channel or other feature, always being at least ca. 1 km apart from each other.

Field surveys

During field surveys in July 2019, we laid six 20-m transects parallel to the shore at each meadow, with three upper intertidal transects, separated laterally by at least 2 m, at the shoreward edge of continuous eelgrass, and three lower intertidal transects at least 4 m closer to the water. Upper transects at the edge of continuous eelgrass were typically close to the mean lower low water height. To assess disease impacts, we sampled eelgrass shoots at each meter along the transects by harvesting the third-rank (third-youngest) eelgrass leaf as representative of disease status of the shoot. Leaves were trimmed by hand at the top of the sheath bundle. At the OR meadows, where eelgrass shoots commonly have only four leaves compared to five or more elsewhere, third-rank leaves are often on the outside of the sheath bundle and carry high epiphyte loads, making it difficult to clean the leaves for imaging. Wasting disease infection rates did not differ significantly between second- and third-ranked leaves at the OR sites (Supporting Information Fig. S1);

we therefore sampled second-rank leaves in OR. Harvested leaves were stored in unfiltered seawater on ice until processing (within 4–6 h of sampling).

To characterize meadows, we measured shoot densities in four replicate quadrats (0.0625–0.36 m²) at 4-m intervals along each transect; we also collected five intact shoots from 4-m intervals to measure shoot morphologies and epiphyte load. During the analysis of disease signs, we imaged the third-rank leaves of these intact shoots, for a total of 120 leaves collected for disease analysis at each site.

Eelgrass metrics

In the lab, we measured sheath length and canopy height (sheath length plus longest leaf length) of the intact shoots, and we assessed epiphyte load by scraping epiphytes from the third-rank leaf onto a preweighed foil tin and drying at 60°C until constant mass. Using the third-rank leaves, we created high-resolution images for analysis of disease prevalence (presence or absence of lesion tissue on an eelgrass leaf), lesion area, and disease severity (proportion of leaf area damaged by lesions). After scraping the leaves to remove epiphytes, we placed the leaves between two sheets of transparent plastic film, scanned the sheets at 600 dpi using an Epson Perfection V550 scanner, and saved the high-resolution images in TIFF format. In most cases, we scanned each entire eelgrass leaf by separating it into multiple fragments and placing the fragments side-by-side on the plastic film (Fig. 1b). To reduce processing time of large leaves (length > 1 m), we excluded visually healthy tissue from the scans; this was done conservatively so that we scanned all areas of visually damaged tissue, including nonwasting disease damage. For this subset of samples, we measured total leaf area (leaf length and width) by hand before separating the diseased tissue for scanning. We also excluded leaves that were entirely visually asymptomatic from scanning.

Eelgrass lesion image segmentation application

Components and workflow

The EeLISA system uses a positive feedback loop with three main components: a CNN machine learning module, a labeling web application module, and a data analysis module (Fig. 3). When the user inputs a batch of scanned images for processing, the machine learning module performs image segmentation to classify each pixel as healthy tissue, lesion tissue, or background. The predictions and scans are then sent to a server and stored in a MongoDB database that users can access through the labeling web application module, which is hosted on Amazon Web Services with a public web address. The labeling application visualizes the scans overlaid with EeLISA's predictions and allows users to edit the predictions if necessary. After the user verifies the predictions from EeLISA, the scans and predictions are processed by the data analysis module, which is written in Python 3.7 and uses the Python library SciPy to calculate total leaf area and lesion tissue area for each leaf, tagged with its respective metadata. Corrections to the predictions made by

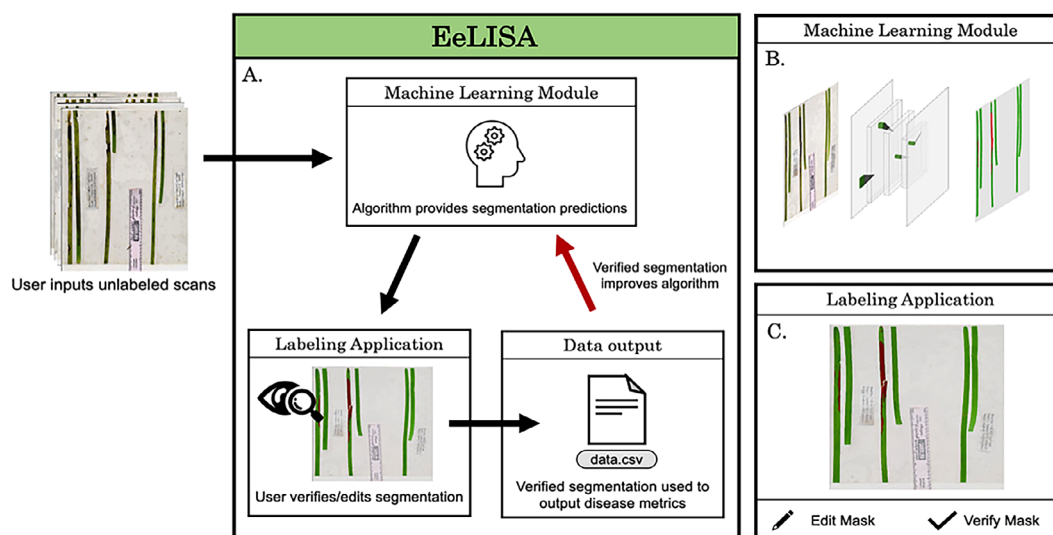


Fig. 3. Schematic of the EeLISA. (a) Diagram of EeLISA's workflow, including the positive feedback loop between the machine learning module, human-computer interaction in the labeling application, and the data analysis module. (b) Schematic of the machine learning module, a fully CNN that takes as input a full scan and outputs a matrix of the same dimensions as the original image, with each pixel classified. (c) Schematic of the labeling application where the user is shown the original scan, overlaid with EeLISA's predictions.

the user can be incorporated by the machine learning module to further train the CNN model, completing the feedback loop. All predictions in this study were made from the same trained and calibrated version of EeLISA, described below.

Development and training

We trained this version of EeLISA using the positive feedback loop described above and a dataset of 1036 eelgrass scans from an earlier study of eelgrass wasting disease in the San Juan Islands, WA (Groner et al. 2021). We divided the dataset into sets of 789 and 247 scans for training and testing sets respectively, and a human processor manually labeled each scan by classifying every pixel as healthy tissue, lesion tissue, or background.

The CNN used to perform the image segmentation was the UNet framework (Ronneberger et al. 2015), which was implemented in the PyTorch deep learning framework. The model was trained on the training set for 40 epochs, using the cross entropy loss and optimized via the ADAM optimizer (Kingma and Ba 2015), with a learning rate of 0.0001 and a batch size of 8. After training, the best performing EeLISA model had an average difference in disease severity with the human labeler of 0.075%. We also assessed the model's performance in terms of average Dice and Jaccard Score, where it scored values of 0.92 and 0.87, respectively. For further details, see Rappazzo et al. (2021).

Calibration

In order to ensure the trained model generalized well to the dataset collected in this study, we compared manual image labels with EeLISA's predictions on a set of 32 calibration scans, with one scan selected randomly from each meadow in the current study. One human expert manually labeled all 32 calibration scans, and two additional human experts labeled a

random subset of 10 calibration scans. The average difference between EeLISA and the human labelers in scoring severity was 1.8% for the full calibration set and 1.5–2% for the subset of 10 calibration scans. These differences were comparable to the differences among the three human labelers (1.1–1.4%), indicating that the trained model generalized to the full dataset.

Analysis of eelgrass wasting disease

After training, we used EeLISA to classify the images of leaves processed during the surveys. We determined disease prevalence by the presence or absence of wasting disease lesions in EeLISA's classifications; total lesion area of each leaf was output directly from EeLISA. We conservatively categorized leaves with $< 2 \text{ mm}^2$ of total lesion area to be asymptomatic, that is, disease was absent, because human experts could not reliably classify damaged areas $< 2 \text{ mm}^2$ during training and calibration. Less than 3% of leaves were in this category. We determined disease severity as the proportion of leaf area covered by lesions using the lesion area and total leaf area measured by EeLISA. For leaves for which only damaged portions of tissue were scanned, we used the hand-measured leaf area to determine severity. Our metric of disease severity is similar to the wasting index proposed by Burdick et al. (1993); however, the wasting index is the maximum percentage of damaged leaf tissue across all leaves on an individual plant whereas in this study we measured severity for the third-rank leaf only. Disease severity of the third-rank leaf is therefore not directly comparable to the plant-level wasting index. We restricted this analysis to third-rank leaves because older leaves with deteriorating tissue and high epiphyte loads could not be reliably cleaned for imaging and because third-rank leaves

integrate environmental conditions over roughly the most recent 2–6 weeks, compared to younger first and second-rank blades (Sand-Jensen 1975).

Verification of pathogen presence

We used qPCR to verify that *L. zosterae* DNA was present in tissue samples with disease signs visually characteristic of eelgrass wasting disease; samples for qPCR were collected at the five meadows in Washington. We further used histological analysis to identify *L. zosterae* cells within diseased plant cells, qualitatively supporting the presence of *L. zosterae* as an infectious agent. Additional details are available in the Supporting Information.

Temperature

We compared eelgrass wasting disease to SST across the study range using 1-km gridded daily SSTs from Group for High-Resolution SST Level 4 analyses, available via NASA's PODAAC portal. This global SST dataset assimilates multisensor satellite data as well as in situ measurements from NOAA iQuam project and meteorological stations. The major SST source was the Multi-Scale Ultra-High Resolution (MUR) product (JPL MUR MEaSUREs Project 2015), with auxiliary data from the Global 1 km SST (G1SST) product (Chao et al. 2009). The coordinates of some meadows fell within the land mask of the SST records; for these sites, we identified the closest ocean pixel within 2 km. The MUR and G1SST products center the 1-km pixels over different points; we accessed both products in order to retrieve SST records for the maximum number of coastal meadows (27 of 32 meadows, Supporting Information Table S1). We excluded one OR meadow, one BB meadow, and three SD meadows from the temperature analysis because they were located in enclosed estuaries and/or distant from the estuary mouth such that the closest ocean pixels were offshore, beyond the estuary areas. The SST values likely did not fully capture thermal variation in the intertidal seagrass meadows; however, comparison between daily SSTs and mean daily in situ temperatures recorded on HOBO MX 2201 temperature loggers (Onset) deployed at each meadow site showed consistent linear relationships (Supporting Information Fig. S3). The SSTs were therefore a reasonable proxy for thermal exposure, and the long-term SST record allowed for calculation of thermal anomalies relative to long-term temperatures.

We retrieved daily SSTs from the MUR and G1SST satellite products for 27 meadows from June 2011 to August 2019. To explore the relationship between temperature and eelgrass wasting disease, we compared meadow-level prevalence, severity, and lesion area to monthly and seasonal mean and maximum temperatures from January to June 2019 (Supporting Information Table S2). Given the spread in local temperatures across the study range (Supporting Information Fig. S2), and the likely adaptation of eelgrass populations to local temperature regimes (Beca-Carretero et al. 2018; King et al. 2018; DuBois et al. 2022), we also calculated relative metrics of anomalies above long-term mean and 90th percentile temperatures. Long-term temperatures

were based on 11-d rolling averages over the 9-yr period of available SST (Hobday et al. 2016). We calculated cumulative positive temperature anomalies as the sum of positive anomalies during each month from January to June 2019 and for 14, 30, 45, 60, and 90 d prior to site-specific sampling dates. Cumulative positive temperature anomaly in June 2019 had a clear and significant correlation with disease prevalence (Supporting Information Table S2), so we selected this relative metric to explore further through statistical modeling.

Statistical analysis

We constructed statistical models of wasting disease prevalence, lesion area, and severity at the scales of meadows, transects, and individual leaves using R (version 4.0.3). For meadows and transects, prevalence was the proportion of diseased leaves out of the total leaves sampled; for leaves, prevalence was the presence or absence of lesions. The predictors in the models were measured at different scales (leaf area at the scale of individual blades, shoot density and epiphyte load at the scale of 20-m transects, and temperature anomaly at the scale of individual meadows). By comparing models across the different scales of analysis, we investigated the relative importance of predictors measured at different scales, to understand if the coarse resolution (1-km) temperatures influenced disease metrics within meadows compared to the finer-resolution seagrass predictors.

For meadows, we used beta regression (Douma and Weedon 2019) and the package *betareg* (Cribari-Neto and Zeileis 2010) to model prevalence and severity as functions of cumulative SST anomaly as a single fixed effect and in combination with leaf area, shoot density, and epiphyte load (Supporting Information Table S3). We used generalized linear mixed models (GLMMs) with gamma distribution to model lesion area, using the package *glmmTMB* (Brooks et al. 2017). For transects and leaves, we constructed models using a hurdle approach (Zuur et al. 2009), with all leaves included in the prevalence models and only leaves with disease signs included in the severity and lesion area models. We used GLMMs with a binomial distribution to model prevalence, mixed-effect beta regression to model severity, and GLMMs with gamma distribution to model lesion area, all using the *glmmTMB* package. We compared models with fixed effects of SST anomaly, leaf area, shoot density, epiphyte load, tidal height (upper or lower), and all interactions between tidal height and other fixed effects to models that excluded interactions and tidal height (Supporting Information Tables S4, S5). We included tidal height as a fixed effect to test whether upper intertidal conditions, likely including increased desiccation and exposure, were associated with greater disease as has been shown in prior work (Groner et al. 2016). For the leaf-level models, we used transect-level means of shoot density and epiphyte load. Random effects were meadow nested within region for transect-level models and transect nested within meadow nested within region for leaf-level models.

Due to the lack of temperature data for five meadows, we ran parallel models, first using data from all 32 meadows and excluding the temperature anomaly effect and second on a restricted dataset from 27 meadows with SSTs and including temperature anomaly as a fixed effect. We compared standardized effect sizes and conditional and marginal R^2 values between models to understand the effect of temperature anomaly and to confirm the restricted dataset did not distort the effects of seagrass metrics compared to the full dataset. For all model sets, we determined best-fitting models using AIC and Akaike weight (Zuur and Ieno 2016) and validated models with residual simulations using the *DHARMA* package (Hartig 2020). We considered effects significant for $p < 0.05$.

Results

Temperature and disease at the meadow scale

Across the study range, wasting disease prevalence and lesion area increased with cumulative positive temperature anomalies. Daily anomalies ranged from -3.6°C to 2.5°C across meadows and cumulative positive anomalies over the month of June ranged from 0°C to 24.1°C (Fig. 4). Both cumulative anomaly in June and leaf area were significant predictors of meadow-wide disease prevalence in July (Fig. 5a,b), together explaining 33% of variation (Supporting Information Table S8), but leaf area had a much smaller effect size (Supporting Information Fig. S4). For lesion area, temperature anomaly was significant while leaf area was not, together explaining 22% of variation (Fig. 5c,d; Supporting Information Table S8). For disease severity, leaf area was a significant predictor but temperature anomaly was not together explaining 43% of variation (Fig. 5e,f; Supporting Information Table S8). Similarly, temperature anomaly was a significant predictor of prevalence and lesion area but not severity for transect- and leaf-level models (Supporting Information Figs. S5, S6). One meadow (BB-E) appears as an outlier, with a high cumulative temperature anomaly yet low disease prevalence; thermal and saline stratification at this low-inflow estuary site may account for this difference (Hearn and Largier 1997). Excluding this meadow, we found a stronger link between meadow-scale prevalence and temperature anomaly (pseudo- $R^2 = 0.49$).

In contrast to the significant link between warm temperature anomalies and wasting disease, we found no associations between absolute temperature metrics in winter, spring, or summer and disease in summer (Supporting Information Table S2). Across the meadows, daily winter temperatures ranged from 5.3°C to 16.1°C , daily spring temperatures ranged from 6.3°C to 19.5°C and daily summer temperatures ranged from 10.8°C to 22.6°C (Supporting Information Fig. S2).

Wasting disease across latitudes

Wasting disease prevalence, severity, and lesion area varied substantially without any strong latitudinal trend (Fig. 6). Between regions, prevalence was highest in WA (70%) and

lowest in OR (20%); however, there was considerable variation within regions (e.g., prevalence ranged from 11% to 92% across the six BB meadows). Disease severity was less variable than prevalence between regions but again varied substantially within regions (e.g., severity ranged from 2% to 31% across the five WA meadows). Lesion area was highest in WA and BB and lowest in OR and SD.

Temperature and disease at transect and leaf scales

Across the transect- and leaf-level models, cumulative SST anomaly had a larger standardized effect size on disease prevalence than any seagrass metric, except for shoot density in the leaf-level model of lesion area (Supporting Information Figs. S5, S6). Models that included cumulative anomaly as a predictor explained more variation in prevalence and lesion area than models with only eelgrass metrics (higher marginal R^2), and models with eelgrass metrics alone explained little variation in prevalence compared to random effects of location. Eelgrass metrics explained a moderate amount of variation in disease severity (Supporting Information Table S8). Shoot density had a consistent positive correlation with prevalence and lesion area and was positively correlated with severity at the leaf level. Leaf area had a consistent negative correlation with severity, a consistent positive correlation with lesion area, and was positively correlated with prevalence at the leaf level. Epiphyte load had a positive correlation with severity at the leaf level (Supporting Information Fig. S6). Tidal height did not directly affect disease metrics, but did interact with shoot density, likely due to peak shoot densities along upper intertidal transects at two sites in BC (Supporting Information Figs. S7, S9).

Application of EeLISA to identify eelgrass wasting disease

EeLISA accelerated the workflow of disease detection by more than 5000 \times and eliminated the need for a trained human expert at every sampling site. Image processing time using EeLISA was less than 5 min, whereas a conservative estimate of human expert processing time, based on prior studies without EeLISA (Groner et al. 2016; Dawkins et al. 2018), would be 7 min per leaf, or 432 h for the complete dataset of 3702 leaves. Calibration testing showed that EeLISA produced image segmentation comparable to a human expert using novel images drawn from all study regions. Eelgrass shoot morphology varied substantially across regions (Supporting Information Fig. S10), and EeLISA's success across variation of three orders of magnitude in leaf area, and across the irregularities in images prepared by > 20 personnel, demonstrates the power and flexibility of this application.

Verification of pathogen presence

Positive amplification of *L. zosterae* DNA from diseased tissue samples confirmed the presence of this pathogen in lesion tissue samples, and positive identification of *L. zosterae* cells in histological samples qualitatively indicated the presence of the pathogen within plant cells (Supporting Information

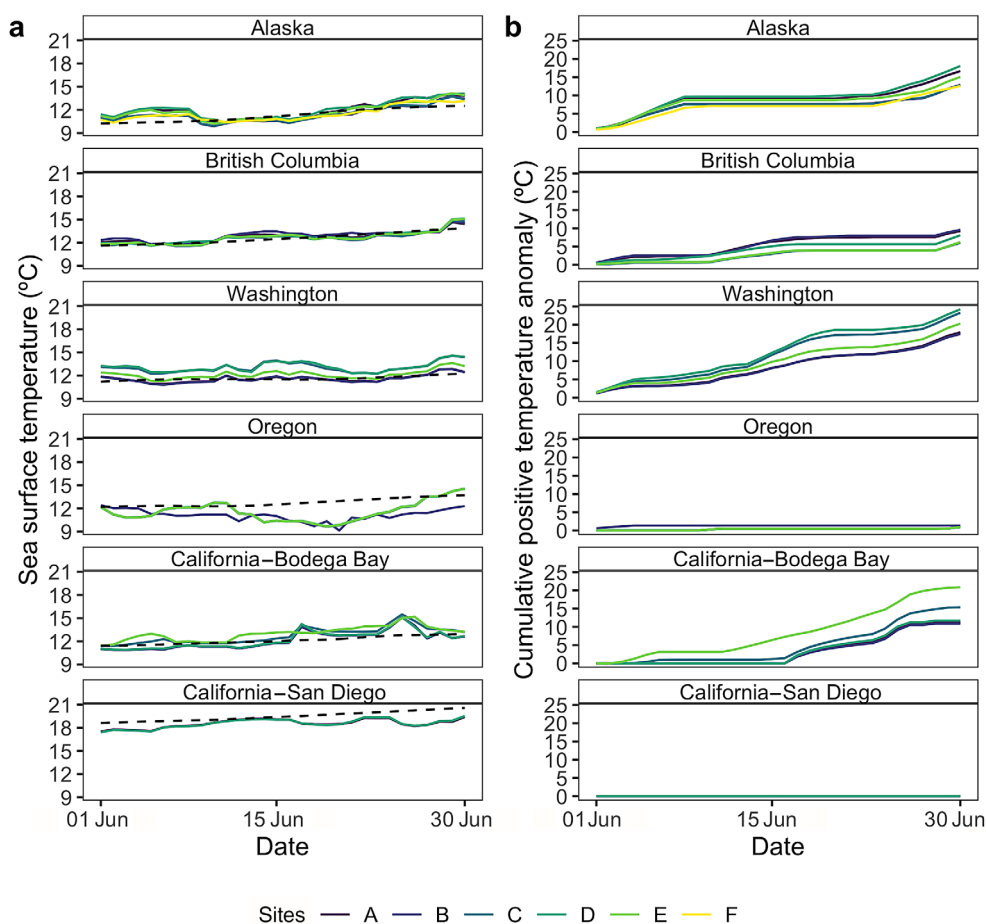


Fig. 4. Daily SSTs and anomalies for June 2019. Daily SSTs (**a**) ranged from $\sim 12^{\circ}\text{C}$ to 20°C across the study range in June 2019. Solid lines show site-specific temperature records, dashed black lines show the regional long-term mean temperature. Cumulative positive temperature anomaly (**b**) in June 2019 reached maximum values of $\sim 24^{\circ}\text{C}$ (over 30 d) for sites in Alaska and Washington. Daily temperature anomalies were calculated relative to site-specific long-term means and summed over the month of June.

Table S9). Together, the qPCR and histology indicated that lesions visually identified as eelgrass wasting disease were signs of infection by *L. zosterae*, supported by prior studies that confirmed *L. zosterae* infection in field-identified lesion tissue at several of our study sites in WA and OR (Groner et al. 2016; Yoshioka et al. 2019).

Discussion

By leveraging AI to conduct rapid and standardized surveys, we quantified eelgrass wasting disease at an unprecedented spatial scale from southeast Alaska to southern California, and we linked disease prevalence and lesion area to warm temperature anomalies across latitudes. In our analysis, absolute temperature and geographical region were not significant predictors of disease, indicating that disease is not a problem restricted to populations at geographic range limits or those at warmest latitudes. Indeed, our findings suggest that the risk of eelgrass wasting disease outbreaks will increase with climate-induced warming throughout the entire range of eelgrass.

A key finding from this study is that the cumulative positive temperature anomaly in the month of June was the strongest predictor of infections in July. This suggests an accumulating negative impact of the warm anomaly on eelgrass performance, as has been documented in mesocosm experiments (Reynolds et al. 2016; Saha et al. 2020). A cumulative temperature effect may explain why laboratory incubations have not generally shown a strong effect of elevated temperature on wasting disease infection, as experimental *L. zosterae* inoculation typically occurs within a day of temperature treatments (Dawkins et al. 2018; Brakel et al. 2019). The cumulative anomaly effect further demonstrates that temperatures do not have to be extreme to cause negative impacts (Reynolds et al. 2016; DuBois et al. 2020), including a negative carbon balance in the plant (Lee et al. 2007; Nguyen et al. 2021). Warming increases growth of the pathogen (Dawkins et al. 2018), reduces the availability of resources for plant immune response (Vergeer et al. 1995), and may impact eelgrass–*L. zosterae* interactions indirectly through changes to the eelgrass microbiome (Trevizan Segovia et al. 2021) and

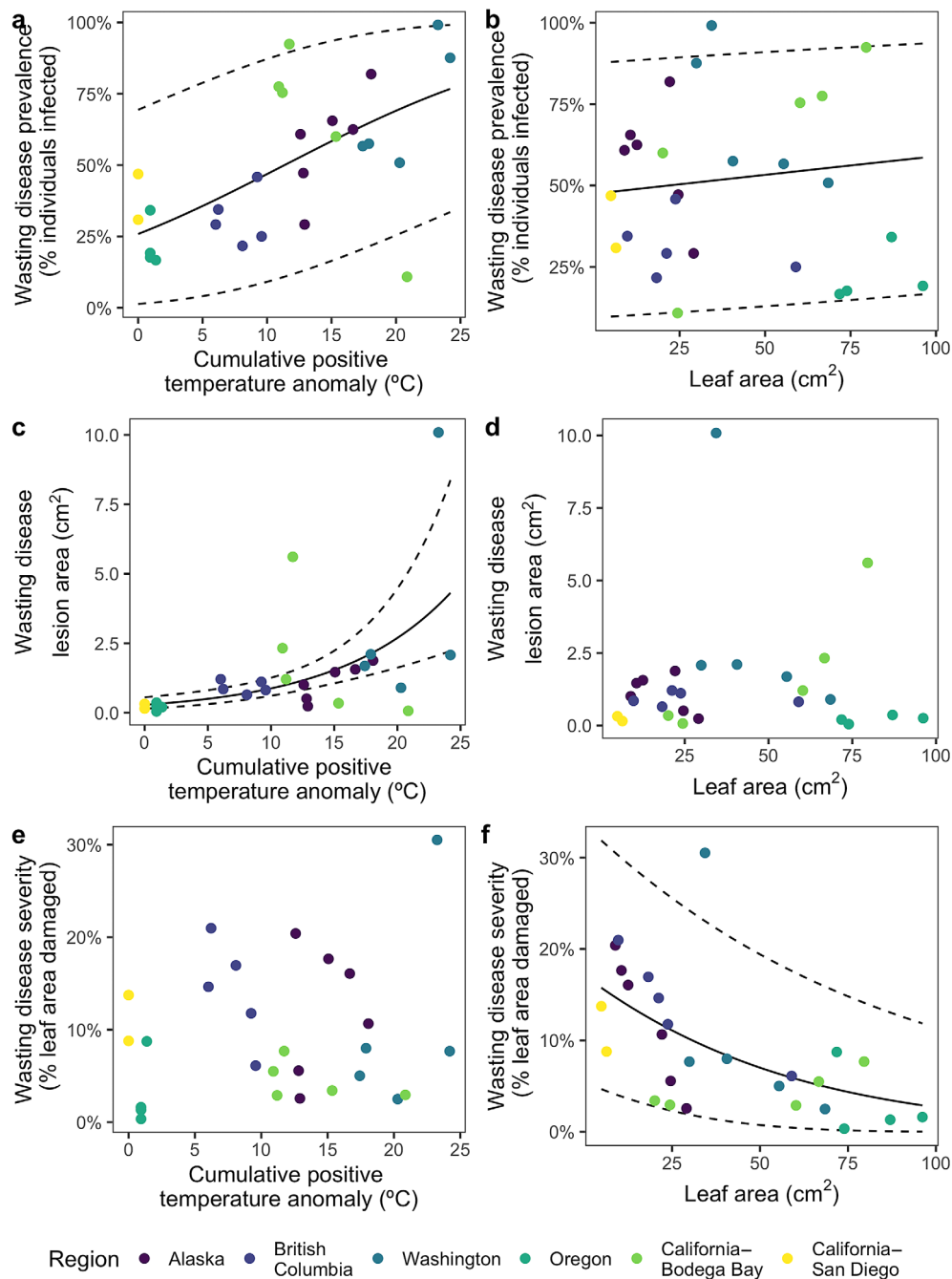


Fig. 5. Effects of cumulative positive temperature anomaly in June and leaf area on wasting disease prevalence, severity, and lesion area at the meadow scale. Both cumulative anomaly in June (**a**) and leaf area (**b**) were significant predictors of wasting disease prevalence. For lesion area, cumulative anomaly was a significant predictor (**c**) and leaf area was not (**d**). For wasting disease severity, cumulative anomaly was not a significant predictor (**e**) whereas leaf area was significant (**f**). Solid lines show simulated model predictions of disease prevalence and severity across the range of the variable of interest while holding the second predictor constant at the median value (median cumulative anomaly was 11.7°C, median leaf area was 29.1 cm²). Dashed lines show the 97.5% and 2.5% quantiles of the simulation. See Supporting Information Fig. S4 for effect sizes and *p*-values.

epifauna grazers (Reynolds et al. 2018). Although we cannot distinguish between these likely simultaneous mechanisms in this study, the overarching relationship between warm water

anomalies and both disease prevalence and lesion area suggests that eelgrass wasting disease will be sensitive to increasing water temperatures from climate change.

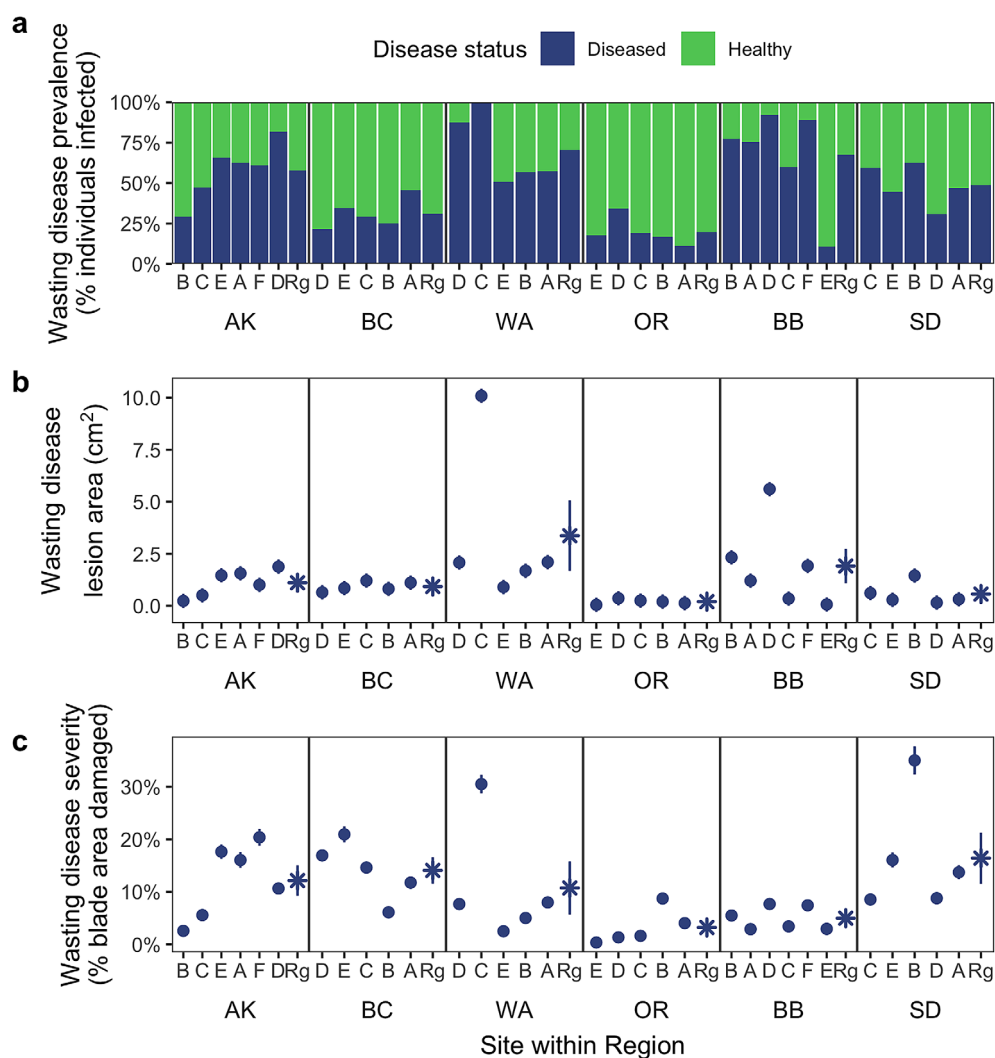


Fig. 6. Wasting disease metrics across the study sites. Wasting disease prevalence (**a**), lesion area (**b**), and severity (**c**) varied between sites and regions with no overarching geographic pattern. Regions are arranged from north (Alaska, AK) to south (California—San Diego, SD) and sites are ordered by latitude within each region. Round points show the site-level mean (\pm SE, $n = 96$ –120 eelgrass leaves), with labels A–F. Stars show the regional means (\pm SE, $n = 5$ –6 meadows), labeled Rg.

The link between increased wasting disease and warm water anomalies, rather than absolute temperature, highlights the importance of eelgrass adaptation to local conditions. Eelgrass is widely distributed, occurring from $\sim 30^{\circ}\text{N}$ to 70°N ; optimal temperatures for growth and photosynthesis vary across this range and generally fall between 15°C and 25°C (Lee et al. 2007). However, populations in different geographic regions occupy distinct thermal niches. Prior work has shown that northern (pole-ward) populations are more sensitive to absolute warming, with plant respiration increasing more rapidly at lower absolute temperatures compared to more southern populations (Beca-Carretero et al. 2018), and that southern (equator-ward) populations recover more quickly from exposure to high absolute temperatures (Franssen et al. 2011; Jueterbock et al. 2016). Our findings emphasize

the importance of relative warming since similar absolute temperatures can represent different intensities of temperature anomalies for distinct eelgrass populations. For example, in 2019, absolute spring temperatures were similar in our British Columbia and Washington sites, and absolute summer temperatures were warmer in British Columbia (Supporting Information Fig. S2), but temperature anomalies, as well as disease metrics, were higher in Washington (Figs. 4, 6). Both genetic adaptation and local acclimation (phenotypic plasticity) likely play a role in these differing responses to thermal stress (Reynolds et al. 2016; King et al. 2018; DuBois et al. 2020). Even at limited spatial scales within our regions, populations of eelgrass separated by less than 20 km exhibit adaptation to local thermal conditions (DuBois et al. 2022). This study connects increases in disease prevalence and lesion area with local

warming regardless of absolute temperature, emphasizing the vulnerability of eelgrass across its geographic range.

Our disease metrics of lesion area and disease severity responded differently to warm temperature anomalies, highlighting the complexity of eelgrass wasting disease dynamics. Below an optimal threshold, warming increases eelgrass growth (Lee et al. 2007); because disease severity standardizes lesion area by leaf area, enhanced plant growth may outpace lesion growth and minimize increases in our measure of severity, despite increased lesion area. Eelgrass also exhibits consistent relative growth rates of 1–2% per day globally, which means that longer leaves grow faster in absolute terms (Ruesink et al. 2018), and the negative correlation between disease severity and blade area shown here and in prior work (Groner et al. 2016, 2021) suggests that eelgrass leaves can outgrow lesions. However, in some cases, possibly when plants are stressed, lesion growth rate can outpace leaf growth (Graham et al. 2021). Furthermore, the positive correlation of lesion area with temperature anomalies suggests that damage to plant tissues from wasting disease will increase with warming. Larger lesion areas will reduce photosynthetic capacity and can damage plant tissue that is not visually infected (Ralph and Short 2002). Infected plants also grow more slowly, and plants with more severe infections can accumulate less sugar in belowground tissues (Graham et al. 2021). Many of the meadows surveyed here may therefore experience negative physiological impacts, with possible consequences for diminished ecosystem function.

Correlations between disease and temperature anomalies indicate the importance of ecosystem-scale environmental conditions. Across the spatial scales of our analysis (meadow, transect, leaf), temperature anomaly measured at the meadow scale (1-km resolution) was a stronger predictor than eelgrass predictors measured at finer scales. Shoot density and leaf area likely increase prevalence of wasting disease and lesion area by increasing direct transmission of the pathogen through contact with diseased tissue (Groner et al. 2016), and in our analysis these plant characteristics were more important to understand wasting disease at smaller spatial scales. Variation in ecosystem-scale environmental conditions other than temperature will also affect eelgrass wasting disease. Abiotic factors such as salinity and light have interactive effects on disease in laboratory studies (Dawkins et al. 2018; Brakel et al. 2019; Jakobsson-Thor et al. 2020) and likely played a role in the 1930s eelgrass wasting disease pandemic (Sullivan et al. 2013). These and additional factors, ranging from nutrient availability to pathogen virulence, were not captured in the surveys and may interact with warming temperatures. Here, we delineate the relationship between localized warming and wasting disease across an unprecedented geographic scale, revealing the urgency for further work, including monitoring over time, to fully characterize the temperature sensitivity of eelgrass wasting disease and to develop forecasting tools.

Surveillance at relevant spatial and temporal scales is critical to successful management and mitigation of disease

(Maynard et al. 2016). EeLISA, the AI system we deployed in this study, facilitates the rapid disease detection necessary for effective surveillance by vastly reducing the time required for image analysis while providing results comparable to a human expert. In marine ecosystems, near real-time monitoring and forecasting tools have been developed for coral bleaching (Liu et al. 2014), but other widely distributed and ecologically disruptive diseases, including dermo in Eastern oysters (Burge et al. 2014), withering syndrome in abalone (Friedman and Finley 2003) and sea-star wasting disease (Harvell et al. 2019) have only been studied retrospectively. EeLISA demonstrates how the application of AI to detect disease outbreaks can accelerate and standardize surveillance for the globally distributed eelgrass wasting disease; this AI system could be expanded to incorporate *Labyrinthula* infections of other seagrass species (Sullivan et al. 2018) and potentially diseases of other marine foundation species, especially those that cause visible changes to coloration of plant tissue, such as bacteria-induced bleaching in macroalgae (Case et al. 2011). More broadly, EeLISA extends recent efforts to apply AI image analysis for detection of crop disease (Mohanty et al. 2016) to marine ecosystems and creates opportunities for streamlined disease surveillance in coastal habitats.

As oceans warm, characterization of temperature–disease relationships is needed to develop forecasting tools to inform management and conservation actions (e.g., as for coral bleaching, Liu et al. 2014; Maynard et al. 2016). By documenting correlations between disease metrics and warm water anomalies across a broad geographic range, our results improve understanding of the temperature sensitivity of eelgrass wasting disease. By identifying a relevant temperature metric, cumulative anomaly in June, these results can inform future efforts to predict outbreaks. Similar metrics that integrate temperature exposure over time are used in agronomy to time pest control interventions (e.g., degree-days, Knutson and Ree 2019); in marine systems, integrated exposure metrics for low pH to can support timing of interventions in commercial oyster hatcheries to mitigate effects of ocean acidification (Gimenez et al. 2018). Although interventions to treat eelgrass wasting disease outbreaks have not yet been developed, tracking these outbreaks is a valuable first step as a sentinel for impending bed decline. Meadows with high disease levels will benefit from management actions that improve growing conditions by minimizing non-disease stressors (e.g., through improved water quality, protection from boat anchoring) and thus provide a better environment for seagrass to resist both disease and temperature stress. Identification of eelgrass populations that are particularly vulnerable to disease, based in part on exposure to warming, can guide prioritization of conservation effort, similar to approaches in coral reef management (Beeden et al. 2012; Darling et al. 2019).

Anthropogenic climate change is increasing positive SST anomalies (Laufkötter et al. 2020), which in turn can increase

disease across taxa (Burge et al. 2014). Climate warming is a major threat to seagrasses (Duarte et al. 2018) and this large-scale study demonstrates that local warming will increase disease risk for eelgrass populations across the species' range, not just for edge-of-range populations. The advances presented here, including the ability to rapidly detect disease signs using AI for image analysis and the application of global SST data to characterize temperature-disease relationships, can provide a foundation for understanding, monitoring, and predicting marine disease dynamics under climate change. As warming increases the risk of outbreaks, new technologies that enable disease surveillance and forecasting at geographic scales will be key to preserving coastal ecosystems and the essential social and economic benefits they provide.

Data availability statement

Data and code for this paper are available at doi: [doi:10.5281/zenodo.4776958](https://doi.org/10.5281/zenodo.4776958).

References

- Aronson, R. B., and W. F. Precht. 2001. White-band disease and the changing face of Caribbean coral reefs, p. 25–38. *In* J. W. Porter [ed.], *The ecology and etiology of newly emerging marine diseases*. Springer.
- Beca-Carretero, P., B. Olesen, N. Marbà, and D. Krause-Jensen. 2018. Response to experimental warming in northern eelgrass populations: Comparison across a range of temperature adaptations. *Mar. Ecol. Prog. Ser.* **589**: 59–72. doi:[10.3354/meps12439](https://doi.org/10.3354/meps12439)
- Beeden, R., J. A. Maynard, P. A. Marshall, S. F. Heron, and B. L. Willis. 2012. A framework for responding to coral disease outbreaks that facilitates adaptive management. *Environ. Manage.* **49**: 1–13. doi:[10.1007/s00267-011-9770-9](https://doi.org/10.1007/s00267-011-9770-9)
- Bockelmann, A.-C., V. Tams, J. Ploog, P. R. Schubert, and T. B. H. Reusch. 2013. Quantitative PCR reveals strong spatial and temporal variation of the wasting disease pathogen, *Labyrinthula zosterae* in Northern European eelgrass (*Zostera marina*) beds. *PLoS One* **8**: e62169. doi:[10.1371/journal.pone.0062169](https://doi.org/10.1371/journal.pone.0062169)
- Brakel, J., S. Jakobsson-Thor, A.-C. Bockelmann, and T. B. H. Reusch. 2019. Modulation of the eelgrass–*Labyrinthula zosterae* interaction under predicted ocean warming, salinity change and light limitation. *Front. Mar. Sci.* **6**. doi:[10.3389/fmars.2019.00268](https://doi.org/10.3389/fmars.2019.00268)
- Brooks, M., and others. 2017. glmmTMB balances speed and flexibility among packages for zero-inflated generalized linear mixed modeling. *R J* **9**: 378. doi:[10.32614/RJ-2017-066](https://doi.org/10.32614/RJ-2017-066)
- Burdick, D., F. Short, and J. Wolf. 1993. An index to assess and monitor the progression of wasting disease in eelgrass *Zostera marina*. *Mar. Ecol. Prog. Ser.* **94**: 83–90. doi:[10.3354/meps094083](https://doi.org/10.3354/meps094083)
- Burge, C. A., and others. 2014. Climate change influences on marine infectious diseases: Implications for management and society. *Annu. Rev. Mar. Sci.* **6**: 249–277. doi:[10.1146/annurev-marine-010213-135,029](https://doi.org/10.1146/annurev-marine-010213-135,029)
- Case, R. J., S. R. Longford, A. H. Campbell, A. Low, N. Tujula, P. D. Steinberg, and S. Kjelleberg. 2011. Temperature induced bacterial virulence and bleaching disease in a chemically defended marine macroalga. *Environ. Microbiol.* **13**: 529–537. doi:[10.1111/j.1462-2920.2010.02356.x](https://doi.org/10.1111/j.1462-2920.2010.02356.x)
- Chao, Y., Z. Li, J. D. Farrara, and P. Hung. 2009. Blending sea surface temperatures from multiple satellites and in situ observations for coastal oceans. *J. Atmos. Ocean. Technol.* **26**: 1415–1426. doi:[10.1175/2009JTECHO592.1](https://doi.org/10.1175/2009JTECHO592.1)
- Cribari-Neto, F., and A. Zeileis. 2010. Beta regression in R. *J. Stat. Softw.* **34**: 1–24. doi:[10.18637/jss.v034.i02](https://doi.org/10.18637/jss.v034.i02)
- Darling, E. S., and others. 2019. Social–environmental drivers inform strategic management of coral reefs in the Anthropocene. *Nat. Ecol. Evol.* **3**: 1341–1350. doi:[10.1038/s41559-019-0953-8](https://doi.org/10.1038/s41559-019-0953-8)
- Dawkins, P., M. Eisenlord, R. Yoshioka, E. Fiorenza, S. Fruchter, F. Giammona, M. Winningham, and C. Harvell. 2018. Environment, dosage, and pathogen isolate moderate virulence in eelgrass wasting disease. *Dis. Aquat. Organ.* **130**: 51–63. doi:[10.3354/dao03263](https://doi.org/10.3354/dao03263)
- Douma, J. C., and J. T. Weedon. 2019. Analysing continuous proportions in ecology and evolution: A practical introduction to beta and Dirichlet regression. *Methods Ecol. Evol.* **10**: 1412–1430. doi:[10.1111/2041-210X.13234](https://doi.org/10.1111/2041-210X.13234)
- Duarte, B., and others. 2018. Climate change impacts on seagrass meadows and macroalgal forests: An integrative perspective on acclimation and adaptation potential. *Front. Mar. Sci.* **5**. doi:[10.3389/fmars.2018.00190](https://doi.org/10.3389/fmars.2018.00190)
- DuBois, K., S. L. Williams, and J. J. Stachowicz. 2020. Previous exposure mediates the response of eelgrass to future warming via clonal transgenerational plasticity. *Ecology* **101**: e03169. doi:[10.1002/ecy.3169](https://doi.org/10.1002/ecy.3169)
- DuBois, K., K. N. Pollard, B. J. Kauffman, S. L. Williams, and J. J. Stachowicz. 2022. Local adaptation in a marine foundation species: Implications for resilience to future global change. *Global Change Biol.* **28**: 2596–2610. doi:[10.1111/gcb.16080](https://doi.org/10.1111/gcb.16080)
- Ellison, A. M., and others. 2005. Loss of foundation species: Consequences for the structure and dynamics of forested ecosystems. *Front. Ecol. Environ.* **3**: 479–486. doi:[10.1890/1540-9295\(2005\)003\[0479:LOFSCF\]2.0.CO;2](https://doi.org/10.1890/1540-9295(2005)003[0479:LOFSCF]2.0.CO;2)
- Franssen, S. U., J. Gu, N. Bergmann, G. Winters, U. C. Klostermeier, P. Rosenstiel, E. Bornberg-Bauer, and T. B. H. Reusch. 2011. Transcriptomic resilience to global warming in the seagrass *Zostera marina*, a marine foundation species. *Proc. Nat. Acad. Sci.* **108**: 19276–19281. doi:[10.1073/pnas.1107680108](https://doi.org/10.1073/pnas.1107680108)
- Friedman, C. S., and C. A. Finley. 2003. Anthropogenic introduction of the etiological agent of withering syndrome into

- northern California abalone populations via conservation efforts. *Can. J. Fish. Aquat. Sci.* **60**: 1424–1431. doi:[10.1139/f03-121](https://doi.org/10.1139/f03-121)
- Gimenez, I., G. G. Waldbusser, and B. Hales. 2018. Ocean acidification stress index for shellfish (OASIS): Linking Pacific oyster larval survival and exposure to variable carbonate chemistry regimes. *Element. Sci. Anthrop.* **6**: 51. doi:[10.1525/elementa.306](https://doi.org/10.1525/elementa.306)
- Graham, O. J., L. R. Aoki, T. Stephens, J. Stokes, S. Dayal, B. Rappazzo, C. P. Gomes, and C. D. Harvell. 2021. Effects of seagrass wasting disease on eelgrass growth and below-ground sugar in natural meadows. *Front. Mar. Sci.* **8**. doi:[10.3389/fmars.2021.768668](https://doi.org/10.3389/fmars.2021.768668)
- Groner, M., C. Burge, C. Kim, E. Rees, K. Van Alstyne, S. Yang, S. Wyllie-Echeverria, and C. Harvell. 2016. Plant characteristics associated with widespread variation in eelgrass wasting disease. *Dis. Aquat. Organ.* **118**: 159–168. doi:[10.3354/dao02962](https://doi.org/10.3354/dao02962)
- Groner, M. L., and others. 2016. Managing marine disease emergencies in an era of rapid change. *Philos. Trans. Roy. Soc. B Biol. Sci.* **371**: 20150364. doi:[10.1098/rstb.2015.0364](https://doi.org/10.1098/rstb.2015.0364)
- Groner, M., and others. 2021. Warming sea surface temperatures fuel summer epidemics of eelgrass wasting disease. *Mar. Ecol. Prog. Ser.* **679**: 47–58. doi:[10.3354/meps13902](https://doi.org/10.3354/meps13902)
- Hartig, F. 2020. DHARMa: Residual diagnostics for hierarchical (multi-level / mixed) regression models. <https://CRAN.R-project.org/package=DHARMa>
- Harvell, C. D., and others. 2019. Disease epidemic and a marine heat wave are associated with the continental-scale collapse of a pivotal predator (*Pycnopodia helianthoides*). *Sci. Adv.* **5**: eaau7042. doi:[10.1126/sciadv.aau7042](https://doi.org/10.1126/sciadv.aau7042)
- Hearn, C. J., and J. L. Largier. 1997. The summer buoyancy dynamics of a shallow Mediterranean estuary and some effects of changing bathymetry: Tomales Bay, California. *Estuar. Coast. Shelf Sci.* **45**: 497–506. doi:[10.1006/ecss.1996.0197](https://doi.org/10.1006/ecss.1996.0197)
- Hewson, I., and others. 2014. Dengue virus associated with sea-star wasting disease and mass mortality. *Proc. Nat. Acad. Sci.* **111**: 17278–17283. doi:[10.1073/pnas.1416625111](https://doi.org/10.1073/pnas.1416625111)
- Hobday, A. J., and others. 2016. A hierarchical approach to defining marine heatwaves. *Prog. Oceanogr.* **141**: 227–238. doi:[10.1016/j.pocean.2015.12.014](https://doi.org/10.1016/j.pocean.2015.12.014)
- Jakobsson-Thor, S., J. Brakel, G. B. Toth, and H. Pavia. 2020. Complex interactions of temperature, light and tissue damage on seagrass wasting disease in *Zostera marina*. *Front. Mar. Sci.* **7**. doi:[10.3389/fmars.2020.575183](https://doi.org/10.3389/fmars.2020.575183)
- JPL MUR MEaSUREs Project. 2015. GHRST level 4 MUR global foundation Sea surface temperature analysis. PO. DAAC, a NASA data repository, CA, USA.
- Jueterbock, A., S. U. Franssen, N. Bergmann, J. Gu, J. A. Coyer, T. B. H. Reusch, E. Bornberg-Bauer, and J. L. Olsen. 2016. Phylogeographic differentiation versus transcriptomic adaptation to warm temperatures in *Zostera marina*, a globally important seagrass. *Mol. Ecol.* **25**: 5396–5411. doi:[10.1111/mec.13829](https://doi.org/10.1111/mec.13829)
- King, N. G., N. J. McKeown, D. A. Smale, and P. J. Moore. 2018. The importance of phenotypic plasticity and local adaptation in driving intraspecific variability in thermal niches of marine macrophytes. *Ecography* **41**: 1469–1484. doi:[10.1111/ecog.03186](https://doi.org/10.1111/ecog.03186)
- Kingma, D. P., and J. Ba. 2015. Adam: A method for stochastic optimization. arXiv:1412.6980 [cs]. doi:[10.48550/arXiv.1412.6980](https://doi.org/10.48550/arXiv.1412.6980)
- Knutson, A. E., and B. Ree. 2019. Biology and management of the pecan nut Casebearer (Lepidoptera: Pyralidae). *J. Integrat. Pest Manage.* **10**: 29. doi:[10.1093/jipm/pmz028](https://doi.org/10.1093/jipm/pmz028)
- Laufkötter, C., J. Zscheischler, and T. L. Frölicher. 2020. High-impact marine heatwaves attributable to human-induced global warming. *Science* **369**: 1621–1625. doi:[10.1126/science.aba0690](https://doi.org/10.1126/science.aba0690)
- Lee, K.-S., S. R. Park, and Y. K. Kim. 2007. Effects of irradiance, temperature, and nutrients on growth dynamics of seagrasses: A review. *J. Exp. Mar. Biol. Ecol.* **350**: 144–175. doi:[10.1016/j.jembe.2007.06.016](https://doi.org/10.1016/j.jembe.2007.06.016)
- Liu, G., and others. 2014. Reef-scale thermal stress monitoring of coral ecosystems: New 5-km global products from NOAA coral reef watch. *Remote Sens.* **6**: 11579–11606. doi:[10.3390/rs6111579](https://doi.org/10.3390/rs6111579)
- Maynard, J., and others. 2016. Improving marine disease surveillance through sea temperature monitoring, outlooks and projections. *Philos. Trans. Roy. Soc. B Biol. Sci.* **371**: 20150208. doi:[10.1098/rstb.2015.0208](https://doi.org/10.1098/rstb.2015.0208)
- Mohanty, S. P., D. P. Hughes, and M. Salathé. 2016. Using deep learning for image-based plant disease detection. *Front. Plant Sci.* **7**. doi:[10.3389/fpls.2016.01419](https://doi.org/10.3389/fpls.2016.01419)
- Muehlstein, L. K., D. Porter, and F. T. Short. 1991. *Labyrinthula zosterae* sp. nov., the causative agent of wasting disease of eelgrass, *Zostera marina*. *Mycologia* **83**: 180–191.
- Nguyen, H. M., P. J. Ralph, L. Marín-Guirao, M. Pernice, and G. Procaccini. 2021. Seagrasses in an era of ocean warming: A review. *Biol. Rev.* **96**: 2009–2030. doi:[10.1111/brv.12736](https://doi.org/10.1111/brv.12736)
- Ralph, P., and F. Short. 2002. Impact of the wasting disease pathogen, *Labyrinthula zosterae*, on the photobiology of eelgrass *Zostera marina*. *Mar. Ecol. Prog. Ser.* **226**: 265–271. doi:[10.3354/meps226265](https://doi.org/10.3354/meps226265)
- Rappazzo, B. H., M. E. Eisenlord, O. J. Graham, L. R. Aoki, P. D. Dawkins, D. Harvell, and C. Gomes. 2021. EeLISA: Combating global warming through the rapid analysis of eelgrass wasting disease. *AAAI* **35**: 15156–15165.
- Reynolds, L. K., K. DuBois, J. M. Abbott, S. L. Williams, and J. J. Stachowicz. 2016. Response of a habitat-forming marine plant to a simulated warming event is delayed, genotype specific, and varies with phenology. *PLoS One* **11**: e0154532. doi:[10.1371/journal.pone.0154532](https://doi.org/10.1371/journal.pone.0154532)
- Reynolds, P. L., and others. 2018. Latitude, temperature, and habitat complexity predict predation pressure in eelgrass

- beds across the Northern Hemisphere. *Ecology* **99**: 29–35. doi:[10.1002/ecy.2064](https://doi.org/10.1002/ecy.2064)
- Ronneberger, O., P. Fischer, and T. Brox. 2015. U-Net: Convolutional networks for biomedical image segmentation, p. 234–241. *In* Medical Image Computing and Computer-Assisted Intervention—MICCAI 2015. Springer International Publishing.
- Ruesink, J. L., and others. 2018. Form-function relationships in a marine foundation species depend on scale: A shoot to global perspective from a distributed ecological experiment. *Oikos* **127**: 364–374. doi:[10.1111/oik.04270](https://doi.org/10.1111/oik.04270)
- Saha, M., others. 2020. Response of foundation macrophytes to near-natural simulated marine heatwaves. *Global Change Biol.* **26**: 417–430. doi:[10.1111/gcb.14801](https://doi.org/10.1111/gcb.14801), 2
- Sand-Jensen, K. 1975. Biomass, net production and growth dynamics in an eelgrass (*Zostera marina* L.) population in Vellerup Vig, Denmark. *Ophelia* **14**: 185–201. doi:[10.1080/00785236.1975.10422501](https://doi.org/10.1080/00785236.1975.10422501)
- Short, F. T., L. K. Muehlstein, and D. Porter. 1987. Eelgrass wasting disease: Cause and recurrence of a marine epidemics. *Biol. Bull.* **173**: 557–562. doi:[10.2307/1541701](https://doi.org/10.2307/1541701)
- Sullivan, B. K., T. D. Sherman, V. S. Damare, O. Lilje, and F. H. Gleason. 2013. Potential roles of *Labyrinthula* spp. in global seagrass population declines. *Fungal Ecol.* **6**: 328–338. doi:[10.1016/j.funeco.2013.06.004](https://doi.org/10.1016/j.funeco.2013.06.004)
- Sullivan, B. K., S. M. Trevathan-Tackett, S. Neuhauser, and L. L. Govers. 2018. Review: Host-pathogen dynamics of seagrass diseases under future global change. *Mar. Pollut. Bull.* **134**: 75–88. doi:[10.1016/j.marpolbul.2017.09.030](https://doi.org/10.1016/j.marpolbul.2017.09.030)
- Trevizan Segovia, B., R. Sanders-Smith, E. M. Adamczyk, C. Forbes, M. Hessing-Lewis, M. I. O'Connor, and L. W. Parfrey. 2021. Microeukaryotic communities associated with the seagrass *Zostera marina* are spatially structured. *J. Eukaryot. Microbiol.* **68**: e12827. doi:[10.1111/jeu.12827](https://doi.org/10.1111/jeu.12827)
- UNEP. 2020. Out of the blue: The value of seagrasses to the environment and to people. United Nations Environment Programme.
- Vergeer, L. H. T., T. L. Aarts, and J. D. de Groot. 1995. The “wasting disease” and the effect of abiotic factors (light intensity, temperature, salinity) and infection with *Labyrinthula zosterae* on the phenolic content of *Zostera marina* shoots. *Aquat. Bot.* **52**: 35–44. doi:[10.1016/0304-3770\(95\)00480-N](https://doi.org/10.1016/0304-3770(95)00480-N)
- Yoshioka, R., J. Schram, and A. Galloway. 2019. Eelgrass pathogen *Labyrinthula zosterae* synthesizes essential fatty acids. *Dis. Aquat. Organ.* **135**: 89–95. doi:[10.3354/dao03382](https://doi.org/10.3354/dao03382)
- Zuur, A. F., E. N. Ieno, N. Walker, A. A. Saveliev, and G. M. Smith. 2009. Mixed effects models and extensions in ecology with R. Springer.
- Zuur, A. F., and E. N. Ieno. 2016. A protocol for conducting and presenting results of regression-type analyses. *Methods Ecol. Evol.* **7**: 636–645. doi:[10.1111/2041-210X.12577](https://doi.org/10.1111/2041-210X.12577)

Acknowledgments

The authors thank the volunteers and field crewmembers who assisted with data collection and sample processing across institutions, and the staff at South Slough National Estuarine Research Reserve for providing logistical support for sampling in Oregon. This work was supported by the National Science Foundation (awards OCE-1829921, OCE-1829922, OCE-1829992, OCE-1829890). This is contribution 104 from the Smithsonian’s MarineGEO and Tennenbaum Marine Observatories Network.

Conflict of Interest

None declared.

Submitted 31 August 2021

Revised 21 April 2022

Accepted 30 April 2022

Editor-in-Chief: K. David Hambright